PHYSICAL REVIEW B **91**, 060403(R) (2015)

Simplex valence-bond crystal in the spin-1 kagome Heisenberg antiferromagnet

Tao Liu,[1] Wei Li,[2,3,*] Andreas Weichselbaum,[2] Jan von Delft,[2] and Gang Su[1,†]

[1]*Theoretical Condensed Matter Physics and Computational Materials Physics Laboratory, School of Physics, University of Chinese Academy of Sciences, Beijing 100049, China*

[2]*Physics Department, Arnold Sommerfeld Center for Theoretical Physics, and Center for NanoScience, Ludwig-Maximilians-Universität, 80333 Munich, Germany*

[3]*Department of Physics, Beihang University, Beijing 100191, China*

(Received 25 June 2014; revised manuscript received 21 January 2015; published 23 February 2015)

We investigate the ground-state properties of a spin-1 kagome antiferromagnetic Heisenberg model using tensor-network (TN) methods. We obtain the energy per site $e_0 = -1.410\,90(2)$, with $D^* = 8$ multiplets retained (i.e., a bond dimension of $D = 24$), and $e_0 = -1.4116(4)$ from large-D extrapolation, by accurate TN calculations directly in the thermodynamic limit. The symmetry between the two kinds of triangles is spontaneously broken, with a relative energy difference of $\delta \approx 19\%$, i.e, there is a trimerization (simplex) valence-bond order in the ground state. The spin-spin, dimer-dimer, and chirality-chirality correlation functions are found to decay exponentially with a rather short correlation length, showing that the ground state is gapped. We thus identify the ground state to be a simplex valence-bond crystal. We also discuss the spin-1 bilinear-biquadratic Heisenberg model on a kagome lattice, and determine its ground-state phase diagram. Moreover, we implement non-Abelian symmetries, here spin SU(2), in the TN algorithm, which improves the efficiency greatly and provides insight into the tensor structures.

DOI: 10.1103/PhysRevB.91.060403 PACS number(s): 75.10.Jm, 05.10.Cc, 75.10.Kt

Introduction. Geometrical frustration, as a particularly interesting phenomenon in quantum antiferromagnets, has raised enormous interest recently [1]. It arises when any classical (Ising) spin configuration cannot satisfy simultaneously all the local terms in the Hamiltonian, which leads to a macroscopic degeneracy and thus greatly enhances quantum fluctuations. Frustration might melt semiclassical spin orders (including magnetic or valence-bond order, etc.), driving the system into an exotic quantum state called a quantum spin liquid [2,3]. Some typical frustrated antiferromagnets include the spin-1/2 and spin-1 Heisenberg models on the triangular lattice [4,5], the spin-1/2 J_1-J_2 square [6–10], and the pyrochlore [11] lattices. Among others, the spin-1/2 kagome Heisenberg antiferromagnetic (KHAF) model is one of the most intriguing frustrated models: Its ground state is widely believed to be a spin liquid [12–18], but its nature is still under debate [19].

KHAF models with higher spins [20] are less well studied, despite their physical realizations in experiments, e.g., organic compound m-MPYNN $\cdot$ BF4 [21–26] and $YCa_3(VO)_3(BO_3)_4$ [27], where the measurements reveal a gapped nonmagnetic state with only short-range spin ordering. Interesting variational wave functions have been proposed for the relevant spin-1 KHAF model, for instance, the static or resonating Affleck-Kennedy-Lieb-Tasaki (AKLT) loop state states [28–30], and the hexagon-singlet solid state [31], etc., yielding some preliminary advances towards understanding the nature of the ground state. Notably, Cai *et al.* considered a fully trimerized variational wave function on the kagome lattice [30], with all the spin-1's in each A (or B) triangle forming a singlet (trimerization). However, its corresponding variational energy for the spin-1 KHAF model is $e_0 = -1$ per site, much higher than that of the topologically ordered resonating AKLT-loop state (a quantum equal-weight superposition of all possible AKLT-loop coverings, $e_0 \approx -1.27$) [29]. The nature of the ground state of the spin-1 KHAF model is still an open question.

In this Rapid Communication, we employ state-of-the-art tensor-network (TN) algorithms [32–34] based on the projected entangled-pair state (PEPS) to study the properties of spin-1 KHAF model, and determine the variational ground-state energy as $e_0 \simeq -1.41$ on an infinitely large two-dimensional (2D) lattice [Fig. 1(a)]. Lattice inversion (reflection) symmetry is found to be broken, where the two kinds of triangles (or simplexes) have different energies [Fig. 1(b)]. We thus call the ground state a simplex valence-bond crystal (SVBC). We also consider the spin-1 bilinear-biquadratic (BLBQ) Heisenberg model, and obtain its ground-state phase diagram, where we find an extended SVBC phase and observe a quantum phase transition between the SVBC and ferroquadrupolar phases at $\theta_c \simeq -0.04\pi$. Some of our results were obtained with an SU(2)-invariant implementation of PEPS, coded using the QSpace tensor library [35], which greatly reduces the costs (see the Supplemental Material [36]).

Model and method. We consider the quantum spin-1 KHAF model with only nearest-neighbor isotropic exchange interactions [i.e., Hamiltonian (1) with $\theta = 0$]. We use the PEPS as a wave-function ansatz [37], and invoke an imaginary-time evolution (through the Trotter-Suzuki decomposition [38]) for optimizations. The initial hexagonal TN [Fig. 1(a)] consists of tensors T_A and T_B, associated with all A and B triangles of the lattice, respectively. Such a TN ansatz has also been employed to study the spin-1/2 KHAF model [16].

After each step of the imaginary-time evolution, we have to reallocate the three physical indices (from T_A to T_B, or the other way round) and truncate the bond state space. Here we use the single-triangle (ST) or double-triangle (DT) update schemes

*w.li@physik.lmu.de
†gsu@ucas.ac.cn

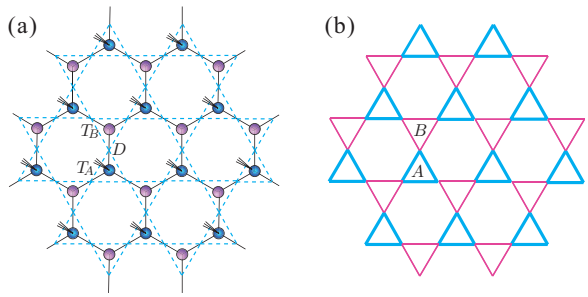

FIG. 1. (Color online) (a) Kagome lattice (dotted lines) and the initial setup of the tensor-network wave function (solid lines). D is the bond dimension, and T_A (T_B) are triangle tensors, with which the physical indices can be associated for convenience. (b) Illustration of the simplex valence-bond crystal. The two kinds of triangles or "simplexes" [of type A (blue) and B (pink)] have different energies, and a lattice inversion symmetry is spontaneously broken.

for truncations (see the Supplemental Material [36]), following Refs. [16,33,34,39]. We find good agreement between ST and DT calculations once the bond dimension D is sufficiently large (see, e.g., Figs. 2 and 5), indicating that ST calculations are sufficient to accurately capture the ground-state properties.

We has also implemented SU(2) symmetry in the TN algorithms, greatly improving the numerical efficiency. To this end, we employed the tensor library QSpace [35], which implements non-Abelian symmetries in TNs in an efficient and transparent framework. We have run data for $D^* = 3$–8, where D^* is the number of multiplets retained on the geometric bonds [see Figs. 3(b) and 3(c)], as compared to the actual number of states D. In the imaginary-time evolution, we only specify the number D^* of retained multiplets, while the representations with respect to SU(2) spin symmetry are free to change

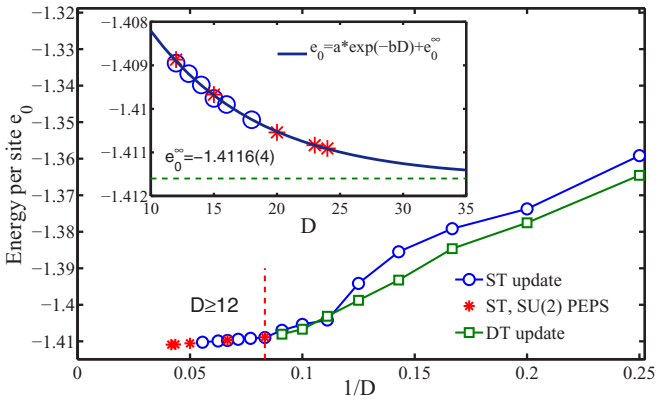

FIG. 2. (Color online) The variational ground-state energy per site e_0 is shown vs $1/D$, obtained from iPEPS contractions [with and without implementing SU(2) symmetry] on the infinite kagome lattice, using both ST and DT update schemes. The inset shows that the $D \geqslant 12$ data (i.e., left-hand side of the dashed line) converge exponentially to the infinite D limit, which is extrapolated as $e_0^\infty = -1.4116(4)$. The convergence of e_0 vs truncation parameters d_c have always been checked (see the Supplemental Material [36]), and the data above are obtained with $d_c = 40$–60 and 100–120 for plain and SU(2) iPEPS contractions, respectively.

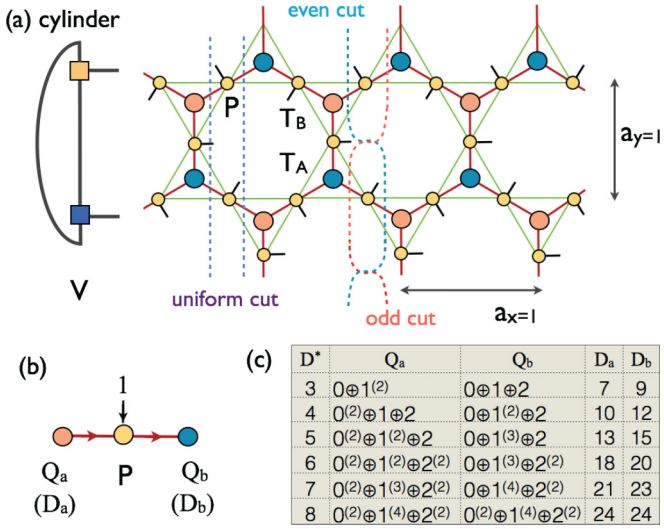

D^*	Q_a	Q_b	D_a	D_b
3	$0\oplus1^{(2)}$	$0\oplus1\oplus2$	7	9
4	$0^{(2)}\oplus1\oplus2$	$0\oplus1^{(2)}\oplus2$	10	12
5	$0^{(2)}\oplus1^{(2)}\oplus2$	$0\oplus1^{(3)}\oplus2$	13	15
6	$0^{(2)}\oplus1^{(2)}\oplus2^{(2)}$	$0\oplus1^{(3)}\oplus2^{(2)}$	18	20
7	$0^{(2)}\oplus1^{(3)}\oplus2^{(2)}$	$0\oplus1^{(4)}\oplus2^{(2)}$	21	23
8	$0^{(2)}\oplus1^{(4)}\oplus2^{(2)}$	$0^{(2)}\oplus1^{(4)}\oplus2^{(2)}$	24	24

FIG. 3. (Color online) (a) Illustration of the cylinders. For XC (YC) geometries, X (Y) direction is with the periodic boundary condition, and length unit $a_x(a_y)$, V is the boundary vector obtained by exact contractions of cylinder PEPS. (b) Implementation of SU(2) symmetry in local tensors: The arrows indicate how the spin multiplets are fused together [40]. The table in (c) shows the specific spin representations $Q_{a,b}$ (and corresponding plain bond dimensions $D_{a,b}$) of the optimized tensors for various D^* (i.e., number of kept bond multiplets). Here $S^{(m)}$ means m multiplets with spin S.

during the optimization process, and eventually converge to the integer ones specified in Fig. 3(c).

Given the optimized tensors [with or without SU(2) symmetry], we consider two geometries for evaluating the expectation values: (a) an infinitely large 2D lattice and (b) an infinitely long cylinder with a finite circumference (Fig. 3). For case (a), we adopt the infinite PEPS (iPEPS) technique [41–43] to contract the double-layer TN, with the boundary matrix product state (MPS) retaining d_c bond states. For case (b), we wrap the TNs on the X or Y cylinders (denoted XC or YC in previous work on kagome cylinders [12,13]), and contract the boundary vector [V in Fig. 3(a)] with a column of tensors, repeating this process until convergence is reached.

Ground-state energy and valence-bond crystal. Figure 2 presents our results of energy per site e_0. The inset shows that e_0's are well converged with retaining $d_c \geqslant 40$ bond states in the boundary MPS. The main panel, where $d_c = 40$, shows that the energy decreases monotonically with increasing bond dimension D, reaching $e_0 = -1.410\,90(2)$ for $D^* = 8$ (i.e., $D = 24$). In the inset of Fig. 2, we find that the $D \geqslant 12$ data are well in the exponential convergence region, and the corresponding fit suggests $e_0^\infty = -1.4116(4)$ in the infinite D limit. This constitutes our best estimate of the ground-state energy in the thermodynamic limit.

In Fig. 4, we show the spin-spin, dimer-dimer, and chiral correlation functions, all evaluated between equivalent sites of two triangles of the same kind, say, A triangles. The spin-spin correlation function is defined by $\langle S_i^z S_j^z \rangle$, and the dimer-dimer one by $\langle D_i D_j \rangle = \langle (S_i^z S_{i+1}^z) \cdot (S_j^z S_{j+1}^z) \rangle - \langle S_i^z S_{i+1}^z \rangle \cdot \langle S_j^z S_{j+1}^z \rangle$, where i and j belong to different triangles. The chiral correlation function is defined as $\langle C_m C_n \rangle =$

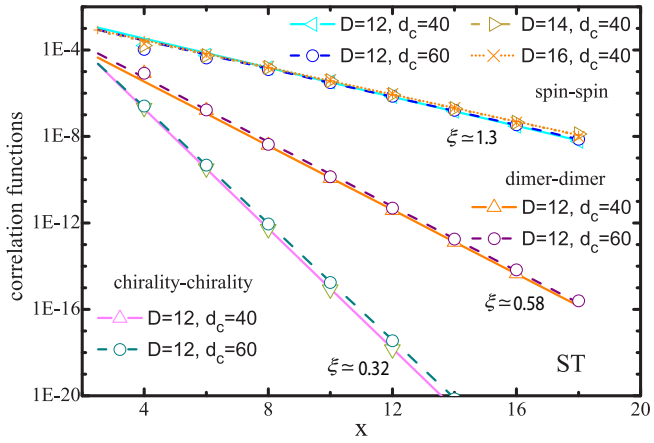

FIG. 4. (Color online) Spatial dependence of various correlation functions (symbols) on a log-linear scale, together with exponential fits $y = c\exp(-x/\xi)$, with ξ indicated with each line. The correlation functions are calculated by iPEPS. x is the distance between triangles with length unit a_x [see Fig. 3(a)]. Note that the square of the converged $\langle S_i^z S_{i+1}^z\rangle \neq 0$ has been subtracted in the definition of dimer-dimer correlations.

$\langle[\mathbf{S}_{m_1}\cdot(\mathbf{S}_{m_2}\times\mathbf{S}_{m_3})][\mathbf{S}_{n_1}\cdot(\mathbf{S}_{n_2}\times\mathbf{S}_{n_3})]\rangle$, where m,n label the positions of two triangles, and m_i,n_i label the positions of the three sites within a triangle. Figure 4 shows that all these correlation functions decay exponentially, implying that the ground state of the spin-1 KHAF model is nonmagnetic and gapped.

Figure 5 shows the energy difference $\Delta E = \frac{2}{3}|E_A - E_B|$ between the A and B triangles, as a function of D. The fact of nonvanishing ΔE means that the ground state spontaneously breaks lattice inversion symmetry. Note that, although our method is initially biased in its treatment of A and B triangles in the ST update, by the end of the projections we reduce the Trotter slice to 10^{-5}, restoring the equivalence between the two kinds of triangles. Besides the ST update, we have also employed the DT update, where the two triangles are treated on equal footing, for determining the ground state. The

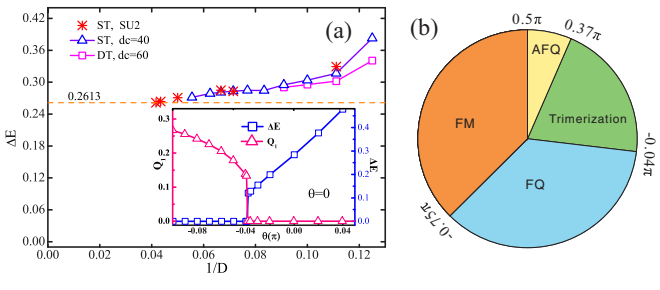

FIG. 5. (Color online) (a) Energy difference between A and B triangles, $\Delta E = 2(E_A - E_B)/3$, where $E_{A(B)} = 9\langle S_i^z S_{i+1}^z\rangle_{A(B)}$, evaluated at the Heisenberg point ($\theta = 0$) with the iPEPS contraction, and plotted vs $1/D$, which show clearly a nonvanishing value ($\delta = \Delta E/e_0 \approx 19\%$ for $D = 24$). The minimal bond dimension needed to capture the SVBC order is $D \gtrsim 7$ [or $D^* = 3$; see the table in Fig. 3(c)]. For smaller D, ΔE vanishes, and hence is not shown here. The inset shows that ΔE vanishes when $\theta < -0.04\pi$, where the ferromagnetic quadrupolar order (Q_1) sets in. (b) Ground-state phase diagram of the spin-1 BLBQ model on the kagome lattice.

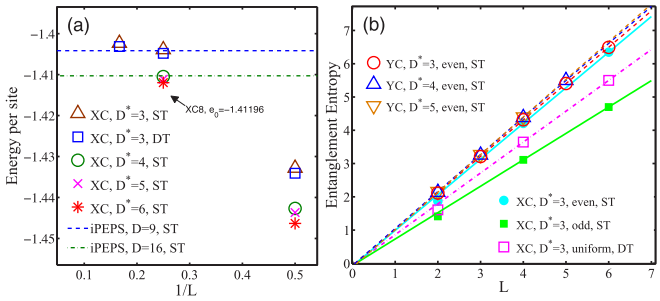

FIG. 6. (Color online) (a) Energy per site and (b) von Neumann entanglement entropies of the tensor-network variational wave functions on cylinders. The X(Y)C geometry is shown in Fig. 3(a), and $L = 2,4,6$ means infinite X(Y)C4, 8, 12 cylinders, respectively.

quantitative agreement between the ST and DT results in Fig. 5 confirm the stability of the spontaneous trimerization order.

Bilinear-biquadratic Heisenberg model. We also studied the spin-1 BLBQ Heisenberg model with the Hamiltonian

$$H = \sum_{\langle ij\rangle}[\cos\theta(\mathbf{S}_i\cdot\mathbf{S}_j) + \sin\theta(\mathbf{S}_i\cdot\mathbf{S}_j)^2], \qquad (1)$$

which recovers the KHAF model when $\theta = 0$. When we tune θ away from the Heisenberg point, we see that the SVBC state belongs to an extended phase. The results are shown in the inset of Fig. 5(a). The energy differences are verified to be robust for various θ's. Interestingly, when we tune θ to the negative side, a phase transition occurs at the transition point $\theta_c \simeq -0.04$, where the trimerization vanishes, and the system turns into a ferroquadrupolar (FQ) phase, with $Q_1 = \langle S_x^2 - S_y^2\rangle \neq 0$.

Figure 5(b) shows the ground-state phase diagram of the spin-1 kagome BLBQ Heisenberg model obtained by exploring other θ values. There are four phases in total: a FQ phase ($-3/4\pi < \theta < -0.04\pi$), a SVBC phase ($-0.04\pi < \theta < 0.37\pi$), an antiferroquadrupolar (AFQ) phase ($0.37\pi < \theta < 1/2\pi$, $\mathbf{Q}_{\rm tot} = \sum_{i\in\triangle}\mathbf{Q_i} = \mathbf{0}$, but $\mathbf{Q_i} \neq \mathbf{0}$), and a ferromagnetic (FM) phase ($1/2\pi < \theta < 5/4\pi$). Note that the SU(3) point ($\theta = \pi/4$) lies in the SVBC phase, thus the SU(3) Heisenberg model also has a trimerized ground state. This observation is in agreement with a previous study of the SU(3) model [44,45]. Note also that Fig. 5(b) is similar to the phase diagram of the spin-1 BLBQ model on a triangular lattice [5], but the antiferromagnetic phase there is replaced by the SVBC phase, and the SU(3) point there is no longer a phase transition point here.

Exact contractions with SU(2) PEPS. The implementation of non-Abelian symmetries leads to a huge numerical gain in efficiency, especially in the contractions of double-layer TNs. For example, we are able to perform exact contractions on a cylinder as large as XC12 for the $D^* = 3$ state, owing to a factor of 340 reduction in the memory (from about 2000 to 6 GB—see the Supplemental Material [36]). A very promising future application would be an iPEPS full update which scales as $D^{10\sim12}$ [41]; due to the very large exponent, the numerical gain from tracking D^* multiplets rather than D individual states per bond can be expected to be huge.

Figure 6(a) shows the energy expectation values up to XC12 ($L = 6$). For the $D^* = 3$ case, the DT offers slightly better energy compared to the ST data. Owing to the implementation

of SU(2) symmetry, we are able to evaluate an optimized $D^* = 6$ state on XC8 ($L = 4$), yielding a variational energy of $e_0 = -1.411\,96$, a variational upper bound of e_0 on a given cylinder, and it agrees well with the iPEPS results in Fig. 2. In addition, trimerization can also be clearly identified in the optimized $D^* = 3,4,5,6$ states, again with a relative difference $\sim 20\%$.

Entanglement entropy. We cut the cylinder PEPS into two halves, and evaluate the von Neumann entropy [46], $S = -\mathrm{Tr}[\rho \log(\rho)]$, fitting it to $S \simeq cL - \gamma$. For the topological states, γ extrapolates to a nonzero constant [14], called the topological entanglement entropy (TEE) [47,48]. Figure 6(b) shows the von Neumann entropies of the $D^* = 3$ states (obtained with ST or DT updates) on XC and YC geometries with $L = 2,4,6$. In the ST update case, owing to the PEPS construction, the cylinder can be cut in two inequivalent ways, called an even or odd cut [see Fig. 3(a)]. In the DT case, where the unit cell tensor is larger, we can cut the cylinder in a uniform way [Fig. 3(a)]. Besides the $D^* = 3$ state, Fig. 3(b) also shows the entanglement entropies of $D^* = 4,5$ states evaluated on various YC geometries; the "even" cut there means the entropies are calculated when the physical indices are associated with T_A in Fig. 3(a). All the entanglement results extrapolate to $\gamma \simeq 0$, suggesting a topologically trivial state.

Conclusions and discussion. We find the ground state of the spin-1 KHAF model to be a gapped SVBC, evidenced by the spontaneous lattice symmetry breaking between two neighboring triangles. An important technical innovation of our work is the explicit implementation of SU(2) symmetry in our PEPS-based algorithms; this not only enhances their numerical performance, but also provides us with useful information about the bond multiplets. To be concrete, the SVBC state and the fully trimerized (trivial) state share some common virtual-spin representations and fusion channels in the tensors. This suggests that the two states are adiabatically connected. In the Supplemental Material [36] we show numerically that this is indeed the case.

Lastly, we address some remarks on the relation to experimental observations. The susceptibility measurements of the organic spin-1 magnet m-MPYNN $\cdot$ BF4 reveal a gapped, nonmagnetic ground state [22–24], consistent with our SVBC picture, which is nonmagnetic and has a spin gap. However, the specific heat measurement shows a round peak at $T/2J' \sim 1/2$ ($2J' \approx 3K$, the coupling strength), suggesting only a short-range ordering. This observation suggests that other complications in the materials (such as next-nearest couplings, distortions, single-ion anisotropy, etc.) should be taken into account, which we leave for a further study.

Note added. Recently, we became aware of three articles, two on a density matrix renormalization group study of the same model [49,50], and the other on a tensor-network study of magnetization curves of the spin-1 kagome model and others [51]. Two of the articles had conclusions consistent with ours [49,51], while the other proposed a different ground state [50]. The striking contrast between the conclusions of Refs. [49,50] suggest that the spin-1 KHAF model constitutes an challenging problem for finite-size DMRG simulations, however, our conclusions based on infinite-size tensor-network simulations do not have such kind of ambiguity.

Acknowledgments. W.L. is indebted to Hong-Hao Tu, Meng Cheng, Shuo Yang, Zi Cai, and Tomotoshi Nishino for stimulating discussions. T.L. thanks Guang-Zhao Qin for his help in polishing the schematic plot. We acknowledge Hong-Chen Jiang and Shou-Shu Gong for discussions about the DMRG calculations of the same model. This work was supported in part by the MOST of China (Grants No. 2012CB932900 and No. 2013CB933401), the Strategic Priority Research Program of the Chinese Academy of Sciences (Grant No. XDB07010100), and NSFC Grant No. 11474249. W.L. was also supported by the DFG through SFB-TR12 and NIM, and acknowledges the hospitality of the Max-Planck Institute for Quantum Optics, where part of the work was performed. A.W. further acknowledges supported by DFG Grant No. WE-4819/1-1.

[1] G. Misguich and C. Lhuillier, in *Frustrated Spin Systems*, edited by H. T. Diep (World Scientific, Singapore, 2005).

[2] P. A. Lee, An end to the drought of quantum spin liquids, Science **321**, 1306 (2008).

[3] L. Balents, Spin liquids in frustrated magnets, Nature (London) **464**, 199 (2010).

[4] S. R. White and A. L. Chernyshev, Neél order in square and triangular lattice Heisenberg models, Phys. Rev. Lett. **99**, 127004 (2007).

[5] A. Läuchli, F. Mila, and K. Penc, Quadrupolar phases of the $S = 1$ bilinear-biquadratic Heisenberg model on the triangular lattice, Phys. Rev. Lett. **97**, 087205 (2006).

[6] H.-C. Jiang, H. Yao, and L. Balents, Spin liquid ground state of the spin-$\frac{1}{2}$ square J_1-J_2 Heisenberg model, Phys. Rev. B **86**, 024424 (2012).

[7] L. Capriotti, F. Becca, A. Parola, and S. Sorella, Resonating valence bond wave functions for strongly frustrated spin systems, Phys. Rev. Lett. **87**, 097201 (2001).

[8] W.-J. Hu, F. Becca, A. Parola, and S. Sorella, Direct evidence for a gapless Z_2 spin liquid by frustrating Néel antiferromagnetism, Phys. Rev. B **88**, 060402(R) (2013).

[9] S.-S. Gong, W. Zhu, D. N. Sheng, O. I. Motrunich, and M. P. A. Fisher, Plaquette ordered phase and quantum phase diagram in the spin-$\frac{1}{2}$ J_1-J_2 square Heisenberg model, Phys. Rev. Lett. **113**, 027201 (2014).

[10] L. Wang, Z.-C. Gu, F. Verstraete, and X.-G. Wen, Spin-liquid phase in spin-1/2 square J_1-J_2 Heisenberg model: A tensor product state approach, arXiv:1112.3331; L. Wang, D. Poilblanc, Z.-C. Gu, X.-G. Wen, and F. Verstraete, Constructing a gapless spin-liquid state for the spin-1/2 J_1-J_2 Heisenberg model on a square lattice, Phys. Rev. Lett. **111**, 037202 (2013).

[11] S. T. Bramwell and M. J. P. Gingras, Spin ice state in frustrated magnetic pyrochlore materials, Science **294**, 1495 (2001).

[12] S. Yan, D. A. Huse, and S. White, Spin-liquid ground state of the $S = 1/2$ kagome Heisenberg antiferromagnet, Science **332**, 1173 (2011).

[13] S. Depenbrock, I. P. McCulloch, and U. Schollwöck, Nature of the spin-liquid ground state of the $S = 1/2$ Heisenberg model on the kagome lattice, Phys. Rev. Lett. **109**, 067201 (2012).

[14] H.-C. Jiang, Z. Wang, and L. Balents, Identifying topological order by entanglement entropy, Nat. Phys. **8**, 902 (2012).

[15] D. Poilblanc, N. Schuch, D. Perez-Garcia, and J. I. Cirac, Topological and entanglement properties of resonating valence bond wave functions, Phys. Rev. B **86**, 014404 (2012); D. Poilblanc and N. Schuch, Simplex $\mathbb{Z}_2$ spin liquids on the kagome lattice with projected entangled pair states: Spinon and vison coherence lengths, topological entropy, and gapless edge modes, *ibid.* **87**, 140407 (2013).

[16] Z. Y. Xie, J. Chen, J. F. Yu, X. Kong, B. Normand, and T. Xiang, Tensor renormalization of quantum many-body systems using projected entangled simplex states, Phys. Rev. X **4**, 011025 (2014).

[17] J. Carrasquilla, Z. Hao, and R. G. Melko, Quantum kagome ice, arXiv:1407.0037.

[18] S.-S. Gong, W. Zhu, and D. N. Sheng, Emergent chiral spin liquid: Fractional quantum Hall effect in a kagome Heisenberg model, Sci. Rep. **4**, 6317 (2014).

[19] Y. Iqbal, F. Becca, S. Sorella, and D. Poilblanc, Gapless spin-liquid phase in the kagome spin-$\frac{1}{2}$ Heisenberg antiferromagnet, Phys. Rev. B **87**, 060405 (2013).

[20] O. Götze, D. J. J. Farnell, R. F. Bishop, P. H. Y. Li, and J. Richter, Heisenberg antiferromagnet on the kagome lattice with arbitrary spin: A higher-order coupled cluster treatment, Phys. Rev. B **84**, 224428 (2011).

[21] K. Awaga, T. Okuno, A. Yamaguchi, M. Hasegawa, T. Inabe, Y. Maruyama, and N. Wada, Variable magnetic interactions in an organic radical system of (*m*-*N*-methylpyridinium α-nitronyl nitroxide) $\cdot X^-$: A possible kagomé antiferromagnet, Phys. Rev. B **49**, 3975 (1994).

[22] I. Watanabe, N. Wada, H. Yano, T. Okuno, K. Awaga, S. Ohira, K. Nishiyama, and K. Nagamine, Muon-spin-relaxation study of the ground state of the two-dimensional $S = 1$ kagomé antiferromagnet [2-(3-*N*-methyl-pyridium)-4,4,5,5-tetramethyl-4,5-dihydro-1H-imidazol-1-oxyl 3-*N*-oxide]BF_4, Phys. Rev. B **58**, 2438 (1998).

[23] N. Wada, T. Kobayashi, H. Yano, T. Okuno, A. Yamaguchi, and K. Awaga, Observation of spin-gap state in two-dimensional spin-1 kagomé antiferromagnet *m*-MPYNN·BF_4, J. Phys. Soc. Jpn. **66**, 961 (1997).

[24] T. Matsushita, N. Hamaguchi, K. Shimizu, N. Wada, W. Fujita, K. Awaga, A. Yamaguchi, and H. Ishimoto, Quantum spin state and magnetization plateaus in an $S = 1$ kagomé Heisenberg antiferromagnet, J. Phys. Soc. Jpn. **79**, 093701 (2010).

[25] G. Lawes *et al.*, Competing magnetic phases on a kagomé staircase, Phys. Rev. Lett. **93**, 247201 (2004).

[26] N. Hamaguchi, T. Matsushita, N. Wada, W. Fujita, and K. Awaga, Specific heat of the spin gapped $S = 1$ kagomé antiferromagnet *m*-MPYNN·BF_4 in magnetic fields, in *Low Temperature Physics: 24th International Conference on Low Temperature Physics - LT24*, edited by Y. Takano *et al.*, AIP Conf. Proc. No. 850 (AIP, Melville, NY 2006), p. 1097.

[27] W. Miller *et al.*, $YCa_3(VO)_3(BO_3)_4$: A kagomé compound based on vanadium(III) with a highly frustrated ground state, Chem. Mater. **23**, 1315 (2011).

[28] H. Yao, L. Fu, and X.-L. Qi, Symmetry fractional quantization in two dimensions, arXiv:1012.4470.

[29] W. Li, S. Yang, M. Cheng, Z.-X. Liu, and H.-H. Tu, Topology and criticality in the resonating Affleck-Kennedy-Lieb-Tasaki loop spin liquid states, Phys. Rev. B **89**, 174411 (2014).

[30] Z. Cai, S. Chen, and Y. P. Wang, Spontaneous trimerization in two-dimensional antiferromagnets, J. Phys.: Condens. Matter **21**, 456009 (2009).

[31] K. Hida, Ground state and elementary excitations of the $S = 1$ kagomé Heisenberg antiferromagnet, J. Phys. Soc. Jpn. **69**, 4003 (2000); Magnetization process of the $S = 1$ and $1/2$ uniform and distorted kagomé Heisenberg antiferromagnets, **70**, 3673 (2001); Ground state phase diagram of the distorted $S = 1$ kagomé Heisenberg antiferromagnets with single-site anisotropy, **71**, 3021 (2002).

[32] H.-C. Jiang, Z.-Y. Weng, and T. Xiang, Accurate determination of tensor network state of quantum lattice models in two dimensions, Phys. Rev. Lett. **101**, 090603 (2008).

[33] W. Li, J. von Delft, and T. Xiang, Efficient simulation of infinite tree tensor network states on the Bethe lattice, Phys. Rev. B **86**, 195137 (2012).

[34] T. Liu, S.-J. Ran, W. Li, X. Yan, Y. Zhao, and G. Su, Featureless quantum spin liquid, $1/3$-magnetization plateau state, and exotic thermodynamic properties of the spin-$1/2$ frustrated Heisenberg antiferromagnet on an infinite Husimi lattice, Phys. Rev. B **89**, 054426 (2014).

[35] A. Weichselbaum, Non-abelian symmetries in tensor networks: A quantum symmetry space approach, Ann. Phys. **327**, 2972 (2012).

[36] See Supplemental Material at http://link.aps.org/supplemental/10.1103/PhysRevB.91.060403 for brief descriptions of the adopted tensor update method, details of the implementation of SU(2) symmetry, and some other supporting data.

[37] F. Verstraete and J. I. Cirac, Renormalization algorithms for quantum-many body systems in two and higher dimensions, arXiv:cond-mat/0407066; V. Murg, F. Verstraete, and J. I. Cirac, Variational study of hard-core bosons in a two-dimensional optical lattice using projected entangled pair states, Phys. Rev. A **75**, 033605 (2007).

[38] In practice, we take the first-order Trotter-Suzuki decomposition [M. Suzuki and M. Inoue, The ST-transformation approach to analytic solutions of quantum systems. I General formulations and basic limit theorems, Prog. Theor. Phys. **78**, 787 (1987); M. Inoue and M. Suzuki, The ST-transformation approach to analytic solutions of quantum systems. II Transfer-matrix and Pfaffian methods, *ibid.* **79**, 645 (1988)] to approximate $e^{-\beta H}$ by the product of a series of evolution gates $e^{-\beta H} = (\prod_{A,B} e^{-\tau h_A} e^{-\tau h_B})^K$, with $K\tau = \beta$, and h_α the three-site triangle Hamiltonian, $\alpha \in \{A, B\}$. In our simulations, we set $\tau = 0.1$ at the beginning, and gradually reduce it to 10^{-5}.

[39] S.-J. Ran, W. Li, B. Xi, Z. Zhang, and G. Su, Optimized decimation of tensor networks with super-orthogonalization for two-dimensional quantum lattice models, Phys. Rev. B **86**, 134429 (2012).

[40] Using the PEPS construction, geometric bonds are associated with auxiliary orthonormal state spaces that can be categorized according to the symmetries of the system. Through tensors, these state spaces are fused with others, as indicated by the arrows with all lines. Since the direction of arrows can be changed throughout the algorithm, there are no arrows shown with the lines in Fig. 3(a). Details will be published elsewhere.

[41] J. Jordan, R. Orus, G. Vidal, F. Verstraete, and J. I. Cirac, Classical simulation of infinite-size quantum lattice systems in two spatial dimensions, Phys. Rev. Lett. **101**, 250602 (2008).

[42] R. Orus and G. Vidal, Simulation of two-dimensional quantum systems on an infinite lattice revisited: Corner transfer matrix for tensor contraction, Phys. Rev. B **80**, 094403 (2009); R. Orus, Exploring corner transfer matrices and corner tensors for the classical simulation of quantum lattice systems, *ibid.* **85**, 205117 (2012).

[43] R. Orus and G. Vidal, Infinite time-evolving block decimation algorithm beyond unitary evolution, Phys. Rev. B **78**, 155117 (2008).

[44] P. Corboz, K. Penc, F. Mila, and A. M. Läuchli, Simplex solids in SU(N) Heisenberg models on the kagome and checkerboard lattices, Phys. Rev. B **86**, 041106(R) (2012).

[45] D. P. Arovas, Simplex solid states of SU(N) quantum antiferromagnets, Phys. Rev. B **77**, 104404 (2008).

[46] J. I. Cirac, D. Poilblanc, N. Schuch, and F. Verstraete, Entanglement spectrum and boundary theories with projected entangled-pair states, Phys. Rev. B **83**, 245134 (2011).

[47] A. Kitaev and J. Preskill, Topological entanglement entropy, Phys. Rev. Lett. **96**, 110404 (2006).

[48] M. Levin and X.-G. Wen, Detecting topological order in a ground state wave function, Phys. Rev. Lett. **96**, 110405 (2006).

[49] H. J. Changlani and A. M. Läuchli, Ground state of the spin-1 antiferromagnet on the kagome lattice, arXiv:1406.4767.

[50] S. Nishimoto and M. Nakamura, Non-symmetry-breaking ground state of the $S = 1$ Heisenberg model on the kagome lattice, arXiv:1409.5870.

[51] T. Picot and D. Poilblanc, Nematic and supernematic phases in kagome quantum antiferromagnets under the influence of a magnetic field, Phys. Rev. B **91**, 064415 (2015).